Improvement of the high-temperature oxidation resistance of Zr alloy cladding by surface modification with aluminum-containing ternary carbide coatings

Chongchong Tang*, Martin Steinbrueck, Mirco Grosse, Sven Ulrich, Michael Stueber, Hans Juergen Seifert
Karlsruhe Institute of Technology (KIT), Institute for Applied Materials (IAM-AWP), Hermann-von-Helmholtz-Platz 1, 76344 Eggenstein-Leopoldshafen, Germany
Corresponding author: Chongchong.tang@kit.edu

Alumina-forming MAX phase ternary carbides are being considered as protective coatings on zirconium alloys as accident tolerant fuel (ATF) cladding because of their resistivity against high-temperature steam oxidation during accident scenarios. This study attempted to synthesize three types of Al-containing MAX phase carbides (Ti_2AlC, Cr_2AlC and Zr_2AlC) as coatings on Zircaloy-4 substrates via deposition of elemental nanoscale multilayer thin films using magnetron sputtering, and subsequent thermal annealing in argon. Formation of Ti_2AlC and Cr_2AlC MAX phases was confirmed after annealing at 800°C and 550°C, respectively, while growth of Zr(Al)C carbide rather than Zr_2AlC MAX phase was observed in the Zr-C-Al system. Oxidation of the three coated samples at 1000°C in steam for 1 hour revealed no protective effect of the Ti_2AlC and Zr(Al)C coatings with significant spallation and cracking. The Cr_2AlC coatings possess superior oxidation resistance and self-healing capability with a thin and dense α-Al_2O_3 layer growth on the surface, which shows good promise as a candidate for coated ATF claddings.

I. Introduction

Zirconium-based alloys, as state-of-the-art cladding material for light water reactors (LWRs), possess a variety of desirable features in steady-state normal operation. However, concerns regarding fast degradation, exothermic reaction with high-temperature steam associated with hydrogen generation in accident scenarios have drawn great attention to developing a more accident-tolerant cladding [1]. The development and deployment of accident tolerant fuel (ATF) claddings for current water-cooled nuclear power reactors became a worldwide interest in the nuclear community latest since the Fukushima accidents [2]. Alternative cladding materials with significantly reduced oxidation kinetics in high-temperature steam environments, for instance FeCrAl alloys and SiC, are being investigated aiming to replace zirconium alloys [3]. Another more near term approach to improve the oxidation resistance is to coat zirconium-based alloy claddings with high-temperature oxidation resistant materials [4].

Materials denominated by the chemical formula $M_{n+1}AX_n$, well-known as MAX phases, represent an extended family of ternary layered, hexagonal carbides and nitrides. Different kinds of chemical bonds co-exist within their layered structure, resulting in their unique attributes combination of both ceramics and metals [5]. Aluminum-containing MAX phase carbides, like Ti_2AlC and Cr_2AlC, possess excellent high-temperature oxidation resistance up to 1400°C in both air and humid atmosphere [6,7]. Their excellent high-temperature oxidation resistance stems from the selective oxidation of aluminum and the small difference of the coefficients of thermal expansion (CTEs) between Al_2O_3 and the substrate leading to growth of an adherent and protective α-Al_2O_3 surface layer during oxidation. In addition, recently intensive irradiation investigations find that the MAX phases are highly irradiation tolerant [8]. Their unique properties provide a great potential for applications in nuclear industry in the form of both bulk and coating.

This study attempted to synthesize three types of MAX phase ternary carbide coatings, namely Ti_2AlC, Cr_2AlC and Zr_2AlC, on Zircaloy-4 substrates. The coatings were deposited by non-reactive magnetron sputtering from three elemental targets applying a nanoscale elemental multilayer design. *Ex-situ* annealing of the as-deposited coatings in argon was performed in order to obtain the MAX phase by solid reaction of the elemental nanoscale multilayers. Single-phase and dense Ti_2AlC and Cr_2AlC MAX phase coatings could be produced while formation of Zr(Al)C rather than MAX phase was confirmed in the Zr-C-Al system. The high-temperature oxidation behavior of three types of coated Zircaloy-4 specimens at 1000°C in steam was tested and compared. The degradation of the coatings during oxidation was investigated by examining the microstructural evolution of the coating-substrate system.

II. Experiment

Square Zircaloy-4 (Zry-4) alloy specimens with sizes of 0.575 × 10 × 10 mm^3 were used as substrates in this study. The chemical composition (wt.%) of the Zircaloy-4 substrates is as follows: Sn ~1.43, Cr ~0.10, Fe ~0.22, O ~1000 ppm, Zr balance. The two main sides of the

Zircaloy-4 specimens were firstly ground with SiC paper, followed by polishing using active oxide polishing suspensions, and finally rinsed with water. The finished average surface roughness (Ra) was around 50 nm. The two polished sides were coated.

A two-step process was developed to synthesize the coatings on Zircaloy-4, namely magnetron sputtering of nanoscale elemental M-C-Al (M: Ti, Zr or Cr) multilayer stacks and subsequent *ex-situ* thermal annealing. The high-temperature oxidation resistance of the coatings relies on the growth of an alumina scale on the surface; however, our previous findings proved that significant diffusion of Al from the coating into the substrate occurred during annealing [9]. In order to suppress the fast diffusion of Al into the substrate and retain the Al reservoir to form alumina scale during high-temperature oxidation, all three coatings have a ~500 nm diffusion barrier. The schematic diagrams of the coatings depicting the elemental nanoscale multilayer stacks and arrangement of the targets and substrates during deposition are shown in Fig. 1. The diffusion barrier was TiC for Ti-based coating, ZrC for Zr-based coating, and Cr metallic layer for Cr-based coatings.

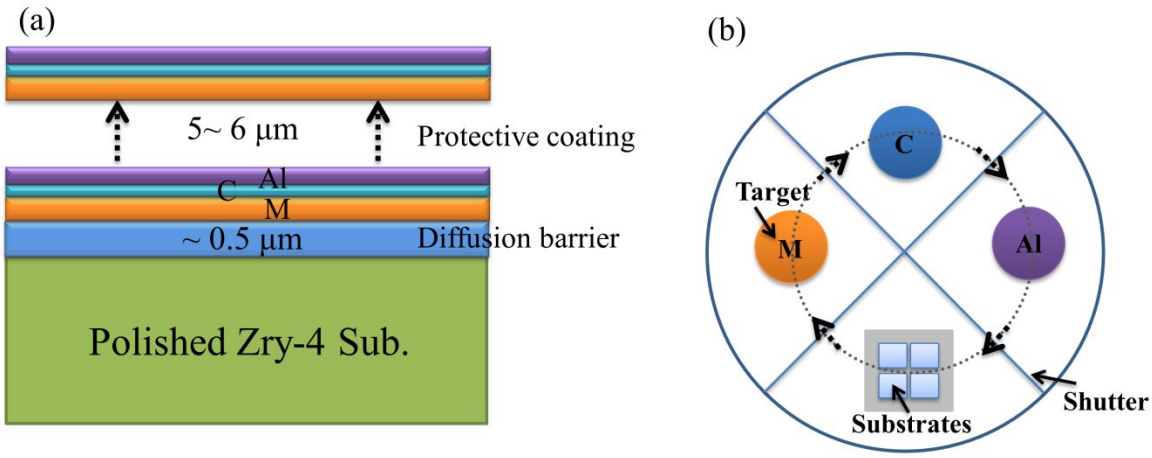

Fig. 1 Schematic of (a) the coatings with the elemental nanoscale multilayer stacks and (b) arrangement of the targets and substrates during deposition.

The M-C-Al multilayer stacks were deposited by non-reactive magnetron sputtering from three elemental targets of titanium, zirconium or chromium, respectively, graphite and aluminum using a laboratory PVD equipment (Leybold Z 550 coater). The thicknesses of each elemental layer are calculated according to the stoichiometric ratio of these three elements in the MAX phases (i.e. 211) and considering their theoretical densities. In addition, the thickest elemental layer, the M layer, was restricted to around 10 nm to reduce the diffusion length during annealing. The substrates were cleaned in an ultrasonic bath with acetone for 10 min. Subsequently, they were fixed on a rotary sample holder at a distance of around 7 cm to the target inside the deposition chamber. Prior to deposition, the chamber was evacuated to a base pressure of around 1×10^{-4} Pa. The substrates were plasma-etched at 500 W RF power in pure Ar atmosphere at 0.5 Pa for 10 min. The working pressure of Ar was maintained at 0.5 Pa during deposition and the substrates were grounded. During multilayer deposition, the PVD equipment runs in a stop-and-go mode. A shutter was installed between the target and the substrate holder to only allow the deposition of one element at each position. Furthermore, the substrates were not additionally heated during deposition. The periodical stack has been repeated until a total film thickness of 5 ~ 6 µm. The diffusion barrier layer was deposited by switching off the Al target power and/or C target power before deposition of the multilayer stacks.

After deposition, the coatings were ex-situ annealed in pure Ar (99.9999%) using a commercial thermal balance (NETZSCH STA-449/409) to yield the potential formation of MAX phases. The heating and the cooling rates were fixed at 10 K/min and the holding time was 10 min. The annealing temperature was 800°C for Ti-based coating, 600°C for Zr-based coating and 550°C for Cr-based coating. The annealing temperatures were chosen based on our previous studies (Ref. 9). The performance of the coatings in high-temperature steam at 1000°C for 1 hour was examined using the thermal balance with a steam furnace. The atmosphere was pure steam with a flow rate of 3 g/h. The uncoated Zircaloy-4 samples were tested at the same conditions for comparison. The crystalline structure of the coatings was analyzed by X-ray diffraction (XRD, Seifert PAD II diffractometer). The surface and cross-section microstructures were investigated using a field-emission scanning electron microscope (SEM, Philips XL30S) equipped with an energy dispersive X-ray spectroscopy (EDS) detector for element analysis.

III. Results and discussions

III.A. Deposition and characterization of the coatings

Fig. 2 shows the XRD patterns of the as-deposited coatings on Zircaloy-4 substrates with respect to the three designs TiCAl, ZrCAl and CrCAl. The sharp diffraction peaks, which were indicated by the symbol Zr in curve(c), obviously stemmed from the Zircaloy-4 substrate. Few additionally broad diffraction peaks with relatively low intensity were observed, and the peaks were identified as Ti, Zr or Cr phase, respectively, for the three designs accompanied with Al phase. The peaks originated from the Zr phase within the coating overlap with the signals of the Zircaloy-4 substrate for the ZrCAl coating. Therefore, the XRD patterns reveal that the transition metal layers and the aluminum layers in the as-deposited coatings are grown in a nanocrystalline structure. The absence of carbon signals indicated that the carbon layers, as expected, are in an amorphous network.

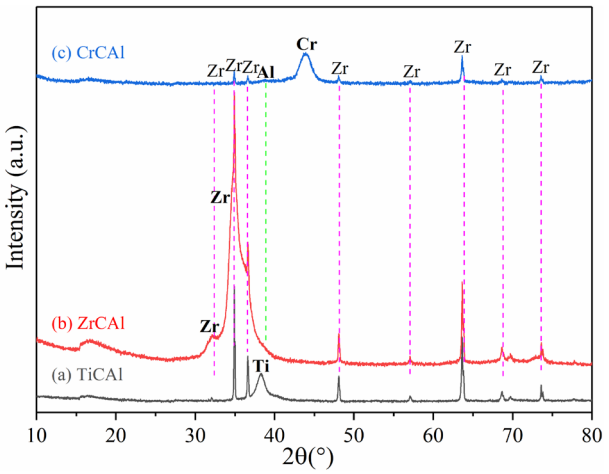

Fig. 2 XRD patterns of the three types of as-deposited coatings on Zircaloy-4 substrates. The peaks originated from coatings are marked with bold symbols.

Fig. 3 displays the XRD patterns of the three types of coatings on Zircaloy-4 substrates after annealing at different temperatures in argon. When comparing Fig. 2 and Fig. 3 (before and after annealing), the XRD patterns show significantly different characteristics: the nanocrystalline transition metal and aluminum phases are not observed anymore and the occurrence of strong (00l) diffraction peaks from the Ti_2AlC and Cr_2AlC MAX phases can immediately be observed for the TiCAl and CrCAl coatings, respectively. Similar to our previous findings, the XRD patterns did not indicate the formation of any intermetallic compound phases in the Ti and Cr ternary systems and Ti_2AlC and Cr_2AlC coatings were successfully fabricated. The TiC and Cr phases found in these two coatings were belonged to the diffusion barrier. Both MAX phase coatings display a basal plane preferred orientation with the *c*-axes perpendicular to the sample surface and the multilayer stacks.

The ZrCAl coatings crystallized in a cubic Zr(Al)C phase with a B1 NaCl crystal structure, rather than Zr_2AlC MAX phase. Al in the annealed coatings is supposed to occupy the lattice position of Zr atoms because of a shift of the diffraction peaks compared to the theoretical values. Annealing of the coatings up to 1200°C resulted in same binary carbide phase.

The phase evolution during annealing of the as-deposited coatings, at least partially, can be interpreted by the thermodynamic stability of the corresponding MAX phases and their counterpart binary carbides. Ti_2AlC and Cr_2AlC are proved to be stable and bulk products have already been obtained several decades ago [10]. However, Al-containing Zr-based MAX phases are often assumed to be unstable or metastable with respect to their competing phases surrounding their compositions [11]. In case of binary carbides, the stability increases in the sequence of CrC_x ($Cr_{23}C_6$, Cr_7C_3 and Cr_3C_2), TiC and ZrC. Therefore, it becomes successively harder converting these binary carbides from Cr to Zr to their corresponding high-ordered MAX phases through reaction with other intermediate phases during annealing. Thus, it seems reasonable that no MAX phase, but Zr(Al)C was formed, in the Zr-C-Al system.

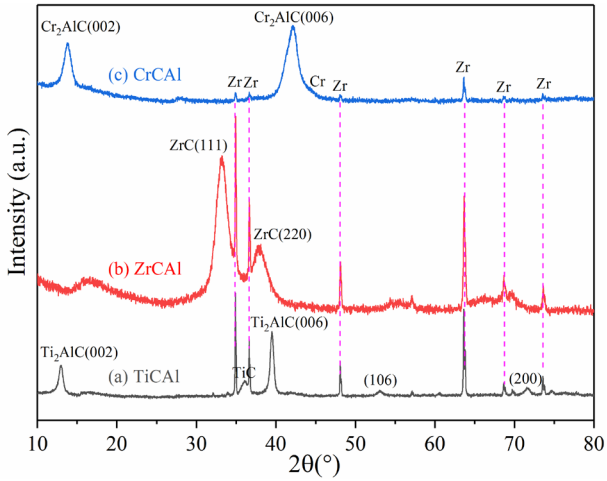

Fig. 3 XRD patterns of the three types of coatings on Zircaloy-4 substrates after annealing at different temperature for 10 min in argon. (a) TiCAl-800°C, (b) ZrCAl-600°C, (c) CrCAl-550°C.

Fig. 4 and Fig. 5 display the SEM micrographs of surface top view and cross-sectional view, respectively, of the three types of coatings on Zircaloy-4 after annealing. All coatings display a uniform and smooth surface without indication of delamination or spallation. However, micro-cracks existed on the surface of the Cr_2AlC coating (Fig. 4(c)), and the two other coatings are

crack-free. The occurrence of the micro-cracks can be explained by the thermal expansion coefficient mismatch between the coatings and the substrate. The linear CTEs of Zircaloy-4 substrate,Ti_2AlC and ZrC are ~6.0×10^{-6} K^1, 8.7×10^{-6} K^{-1} and 6.2×10^{-6} K^{-1}, respectively; whereas the value is 11~13.3×10^{-6} K^{-1} for Cr_2AlC, two times higher than that of substrate. Therefore, the Cr_2AlC coating sustains high magnitude of tensile stress when cool down to normal temperature, leading to crack of the coatings. One solution to eliminate the micro-cracks can be utilization of the as-deposited coatings or searching a more suitable diffusion barrier that can serve as a buffer layer. As shown in Fig. 5, the coatings are dense and free of typical columnar structure owing to the two-step synthesis approach. The 500 nm thick diffusion barriers can be easily distinguished by the different contrast. The total thicknesses were around 5.5 μm for Ti_2AlC and Zr(Al)C coatings, and 6.5 μm for Cr_2AlC coating.

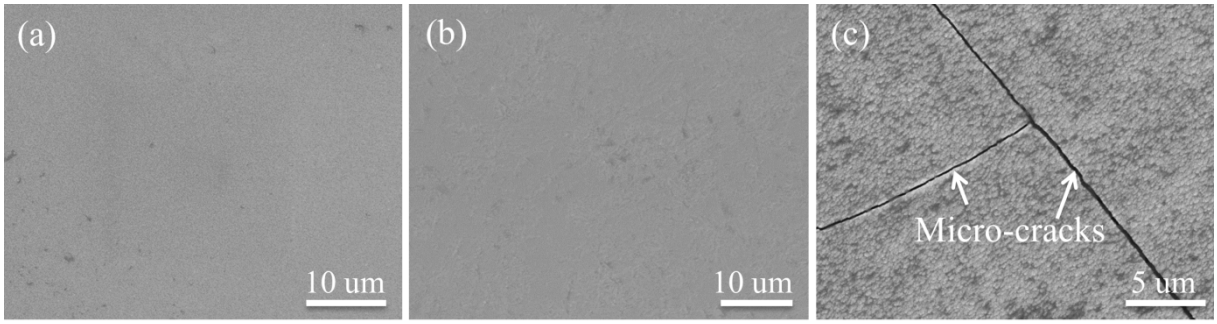

Fig. 4 SEM micrographs of surface top view of the three types of coatings on Zircaloy-4 after annealing. (a) Ti_2AlC coating, (b) Zr(Al)C coating, (c) Cr_2AlC coating.

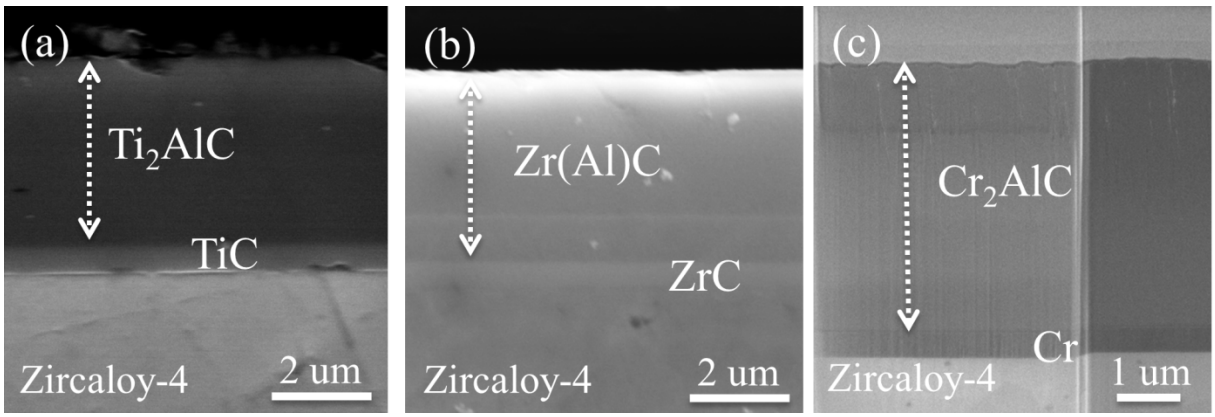

Fig. 5 SEM micrographs of cross-sectional view of the three types of coatings on Zircaloy-4 after annealing. (a) Ti_2AlC coating, (b) Zr(Al)C coating, (c) Cr_2AlC coating. All three coatings have a 500 nm binary carbide or metallic layer as diffusion barrier.

III.B. High-temperature oxidation behavior in steam

Coated coupons together with uncoated Zircaloy-4 as reference were oxidized in pure steam atmosphere at 1000°C for 1 hour to evaluate the oxidation resistance of the three types of coatings. Fig. 6 shows the oxidation kinetics, i.e. mass gain per unit surface area, of the four samples. The uncoated Zircaloy-4 obeyed a parabolic oxidation kinetics and the mass gain reached 25 mg/cm^2 after the exposure. The curves of Ti_2AlC and Zr(Al)C coated samples showed similar oxidation rates during the whole exposure. This indicates that these two coatings failed from the beginning of the oxidation without any oxidation resistance improvement at 1000°C in steam. The Cr_2AlC coated samples displayed excellent oxidation resistance featured by a very low mass gain rate. The final mass gain was ~3.3 mg/cm^2, nearly 8 times lower than that of uncoated Zircaloy-4. Furthermore, the majority of the mass gain was contributed by the uncoated edges which will be shown later.

Fig. 7 are the SEM micrographs of surface top views of the three types of coatings on Zircaloy-4 after oxidation at 1000°C in steam for 1 hour. Significant spallation was observed for Ti_2AlC and Zr(Al)C coatings after the test, and the coatings were completely oxidized identified by EDS. Nearly all Zr(Al)C coating was gone as shown in Fig. 7(b). Oxidation of these two types of coatings at lower temperature (800°C) in steam resulted in formation of an Al_2O_3-rich layer with TiO_2 or ZrO_2 layers beneath for Ti_2AlC and Zr(Al)C coating, respectively,

rather than a dense alumina layer [12,13]. The Cr_2AlC coatings remained adherent without any delamination or spallation (Fig. 7(c)). No accelerated oxidation or nodule formation occurred around the micro-cracks.

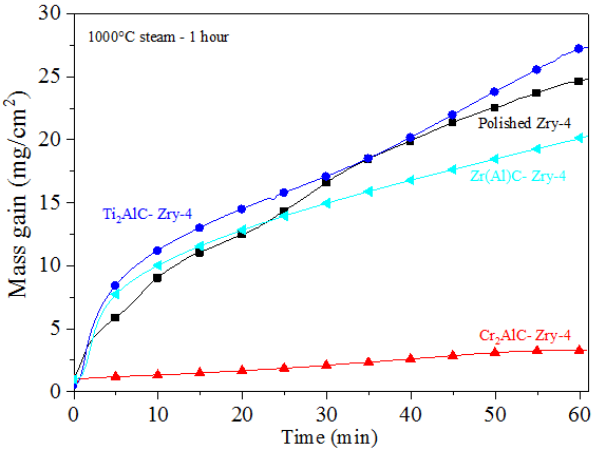

Fig. 6 Oxidation kinetics of the coated and uncoated Zircaloy-4 during oxidation at 1000°C in steam for 1 hour.

Fig. 8 shows the SEM micrographs of cross-sectional views of the Cr_2AlC coated Zircaloy-4 and uncoated Zircaloy-4 after the oxidation test. As illustrated in the overview image Fig. 8(a), the uncoated edges were severely attacked by the steam and a thick, porous ZrO_2 layer formed. Steam penetrated deeply into the matrix through the uncoated edges and limited local failure of the coatings near the edge area was observed. In all other regions, the coatings protected the underneath substrate from oxidation. The high-magnification image at the coating/substrate interface, Fig. 8(b), unambiguously evidences a thin, dense α-Al_2O_3 scale growth on the Cr_2AlC coatings. The α-Al_2O_3 scale suppresses the fast consumption of the coatings during oxidation. Outward diffusion of Al for oxidation resulted in transformation of the Cr_2AlC to binary CrC_x, which is depicted in Fig. 8(b) by the contrast discrepancy of two domains and further ascertained by XRD and EDS (not shown here). Self-healing capability, which has been intensively studied for bulk MAX phases, was inherited by the Cr_2AlC coating herein. As seen in Fig. 8(b), the original micro-cracks were filled by alumina and no obvious internal oxidation of the Zircaloy-4 substrate underneath the cracks was confirmed. The crack-healing behavior was due to high diffusivity of Al in the MAX phase and a sufficient volume expansion associated with oxide (Al_2O_3) formation [14]. Some small voids were observed at the coating/substrate interface and the frontier between the Cr diffusion barrier and Cr_2AlC coating became unnoticeable, which were attributed to the interdiffuion during oxidation.

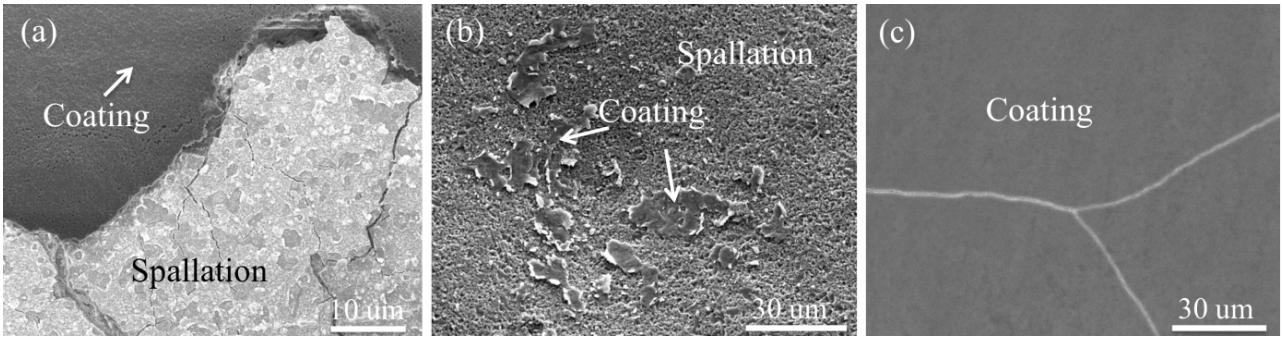

Fig. 7 SEM micrographs of surface top view of the three types of coatings on Zircaloy-4 after oxidation at 1000°C in steam for 1 hour. (a) Ti_2AlC coating, (b) Zr(Al)C coating, (c) Cr_2AlC coating.

Oxidation of uncoated Zircaloy-4 at the same condition led to growth of a porous, non-protective ZrO_2 layer at both sides as in Fig. 8(c). The thickness of this ZrO_2 layer was around 135 μm; in contrast, the alumina layer on Cr_2AlC coating was only ~0.6 μm, which was more than 200 times thinner.

The distinctive performance of the three types of coatings during oxidation at 1000°C in steam can be explained by their oxide scale configuration and microstructure. TiO_2 and ZrO_2 scales have poor performance in high-temperature steam atmosphere with high growth rates. Besides, these two oxides have several polymorphs. Potential phase transformation during oxidation probably make the Ti_2AlC and Zr(Al)C coatings susceptible to cracking and spallation, as shown in Fig. 7. However, Cr_2O_3 and α-Al_2O_3 share similar crystal structure and are completely miscible. Cr_2O_3 can act as nucleation sites for α-Al_2O_3, which will promote and accelerate the growth of alumina during oxidation. Therefore, a thin and dense alumina layer can establish on Cr_2AlC coatings. Thus, Cr_2AlC-based coatings hold good promise as protective coatings on Zr-based alloy claddings to improve the accident tolerance of current water-cooled nuclear reactors.

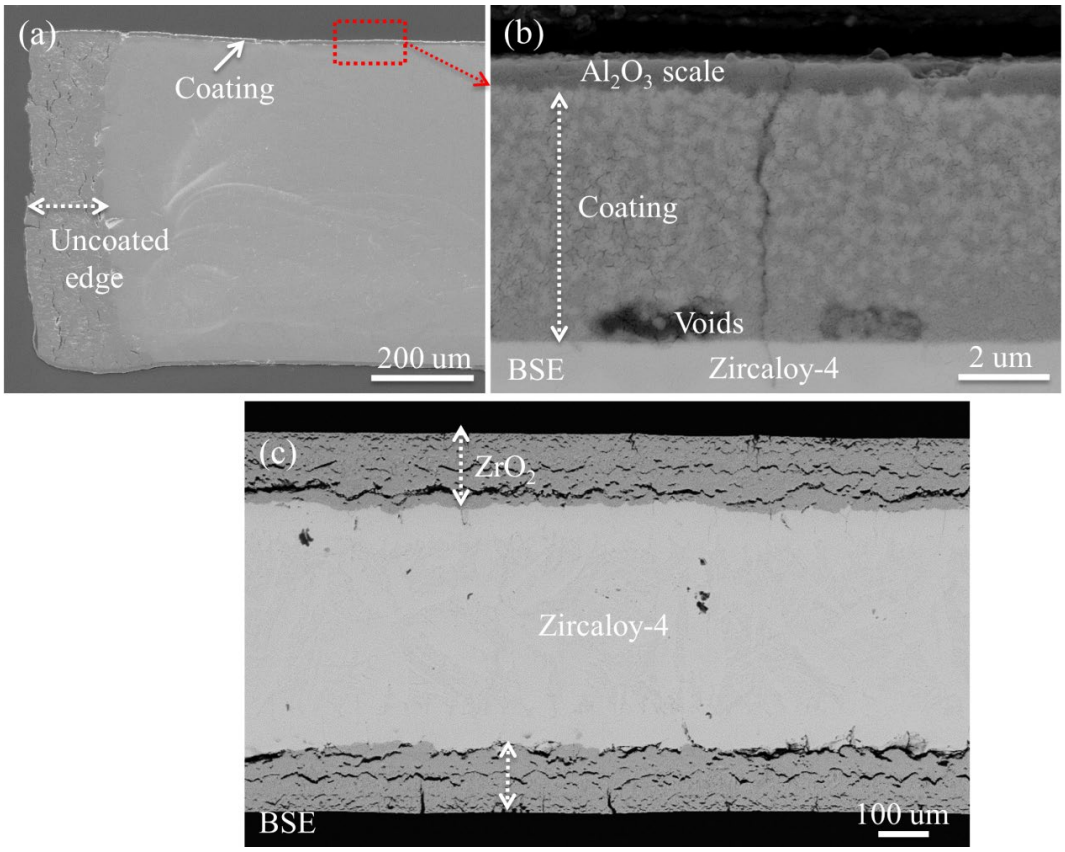

Fig. 8 SEM micrographs of cross-sectional view of Cr_2AlC coated Zircaloy-4 (a) overview image, (b) high-magnification image at coating/substrate interface, and (c) uncoated Zircaloy-4 after oxidation at 1000°C in steam for 1 hour.

IV. CONCLUSIONS

This study attempted to synthesize three types of MAX phase coatings (Ti_2AlC, Cr_2AlC and Zr_2AlC) on Zircaloy-4 substrates as ATF cladding. A two-step approach was adopted, i.e. first deposition of elemental nanoscale multilayer thin films using magnetron sputtering from three elemental targets, and subsequent thermal annealing in argon. The formation of Ti_2AlC and Cr_2AlC MAX phases was confirmed after annealing at 800°C and 550°C for 10 min, respectively, while growth of Zr(Al)C carbide rather than Zr_2AlC MAX phase was observed in the Zr-C-Al system. The coating thicknesses are few microns with a 500 nm binary carbide or metallic layer as diffusion barrier. Micro-cracks were observed in the Cr_2AlC coatings, while the other two coatings are dense and crack-free.

Oxidation of the three coated samples at 1000°C in steam for 1 hour revealed no protective effect of the Ti_2AlC and Zr(Al)C coatings with significant spallation and cracking. Growth of an Al_2O_3-rich layer with TiO_2 or ZrO_2 layer beneath for Ti_2AlC and Zr(Al)C coating, respectively, was confirmed rather than dense alumina layer. The Cr_2AlC coatings possess superior oxidation resistance and self-healing capability with a thin and dense α-Al_2O_3 layer growth on the surface. The thickness of the α-Al_2O_3 layer is ~ 0.6 µm after oxidation, two hundred times thinner than that of ZrO_2 layer formed on uncoated Zircaloy-4. Cr_2AlC-based coatings thus are promising as a candidate for coated ATF claddings. Oxidation test in steam at higher temperatures in company with long exposure time, and autoclave test simulating normal operation for the Cr_2AlC-based coatings are planned in the near future.

ACKNOWLEDGMENTS

This work was supported by the Helmholtz (HGF) programs NUSAFE and STN at the Karlsruhe Institute of Technology. It was further partially carried out with support of the Karlsruhe Nano Micro Facility (KNMF, www.knmf.kit.edu), a Helmholtz research infrastructure at the Karlsruhe Institute of Technology (KIT, www.kit.edu). C. Tang appreciates the PhD fellowship funded by the China Scholarship Council (CSC). The authors also thank the Mr. S. Zils for his technical support during coating deposition.

REFERENCES

1. Steinbrück, M., Große, M., Sepold, L. & Stuckert, J. Synopsis and outcome of the QUENCH experimental program. *Nucl. Eng. Des.* **240,** 1714–1727 (2010).
2. Zinkle, S. J., Terrani, K. A., Gehin, J. C., Ott, L. J. & Snead, L. L. Accident tolerant fuels for LWRs: A perspective. *J. Nucl. Mater.* **448,** 374–379 (2014).
3. Duan, Z. *et al.* Current status of materials development of nuclear fuel cladding tubes for light water reactors. *Nucl. Eng. Des.* **316,** 131–150 (2017).
4. Tang, C., Stueber, M., Seifert, H. J. & Steinbrueck, M. Protective coatings on zirconium-based alloys as accident-tolerant fuel (ATF) claddings. *Corros. Rev.* **35,** 141–166 (2017).
5. Barsoum, M. W. The MN+1AXN phases: a new class of solids; thermodynamically stable nanolaminates. *Prog. Solid State Chem.* **28,** 201–281 (2000).
6. Tang, C., Steinbrück, M., Große, M., Bergfeldt, T. & Seifert, H. J. Oxidation behavior of Ti2AlC in the temperature range of 1400 °C–1600 °C in steam. *J. Nucl. Mater.* **490,** 130–142 (2017).
7. Hajas, D. E. *et al.* Oxidation of Cr2AlC coatings in the temperature range of 1230 to 1410°C. *Surf. Coatings Technol.* **206,** 591–598 (2011).
8. Tallman, D. J. *et al.* Effect of neutron irradiation on select MAX phases. *Acta Mater.* **85,** 132–143 (2015).
9. Tang, C. *et al.* Synthesis and characterization of Ti2AlC coatings by magnetron sputtering from three elemental targets and ex-situ annealing. *Surf. Coatings Technol.* **309,** 445–455 (2017).
10. Jeitschko, W., Nowotny, H. & Benesovsky, F. Carbides of formula T2MC. *J. Less Common Met.* **7,** 133–138 (1964).
11. Lapauw, T. *et al.* Synthesis of the new MAX phase Zr2AlC. *J. Eur. Ceram. Soc.* **36,** 1847–1853 (2016).
12. Tang, C. *et al.* Assessment of high-temperature steam oxidation behavior of Zircaloy-4 with Ti2AlC coating deposited by magnetron sputtering. in *The Nuclear Materials Conference* (2016).
13. Tang, C. *et al.* Evaluation of magnetron sputtered protective Zr-Al-C coatings for accident tolerant Zircaloy claddings. in *2017 Water Reactor Fuel Performance Meeting* 1–9 (2017).
14. Farle, A.-S., Kwakernaak, C., van der Zwaag, S. & Sloof, W. G. A conceptual study into the potential of Mn+1AXn-phase ceramics for self-healing of crack damage. *J. Eur. Ceram. Soc.* **35,** 37–45 (2015).